

Cite this article as: Li Shijiang, Yan Shufang, Chen Weidong, et al. Effect of Cerium Content on Hydrogen Resistance of ZrH<sub>1.8</sub> MAO Coatings[J]. Rare Metal Materials and Engineering, 2022, 51(03): 793-799.

ARTICLE

# Effect of Cerium Content on Hydrogen Resistance of ZrH<sub>1.8</sub> MAO Coatings

Li Shijiang<sup>1</sup>, Yan Shufang<sup>1</sup>, Chen Weidong<sup>1,2</sup>, Ma Wen<sup>1,2</sup>

<sup>1</sup> School of Materials Science and Engineering, Inner Mongolia University of Technology, Hohhot 010051, China; <sup>2</sup> Inner Mongolia Key Laboratory of Thin Film and Coatings Technology, Hohhot 010051, China

**Abstract:** The ceria-stabilized zirconia (CSZ) coating with an excellent hydrogen resistance performance was prepared by micro-arc oxidation (MAO) with cerium addition. The thickness, bonding strength, morphology, phase structure, chemical valence, and hydrogen resistance of ceramic coatings were investigated by coating thickness gauge, auto-scratch tester, scanning electron microscopy, energy dispersive X-ray spectrometer, X-ray diffraction, and X-ray photoelectron spectroscopy, and vacuum dehydrogenation experiment. Results show that CSZ ceramic coatings are mainly composed of monoclinic zirconia (m-ZrO<sub>2</sub>), tetragonal zirconia (t-ZrO<sub>2</sub>), and t-Zr<sub>0.82</sub>Ce<sub>0.18</sub>O<sub>2</sub>. With increasing the cerium content, the thickness of coating is increased. When the cerium content is 9mol%, the thickness of CSZ ceramic coating reaches the maximum of 135.5 μm, the bonding force is 52.46 N, and the hydrogen permeation reduction factor (PRF) is 19, which indicates an excellent hydrogen resistance. The cerium addition inhibits the phase transformation from t-ZrO<sub>2</sub> to m-ZrO<sub>2</sub>, thereby promoting the formation of stable t-ZrO<sub>2</sub> at elevated temperatures.

**Key words:** zirconium hydride; micro-arc oxidation; cerium content; hydrogen permeation reduction factor

Zirconium hydride is one of the ideal neutron moderator materials in small reactors<sup>[1,2]</sup> due to its low neutron absorption cross-section, negative temperature coefficient of reactivity, high stability, and high hydrogen density. However, the zirconium hydride will lose hydrogen from the substrate at the service temperature of 600 °C, which reduces the efficiency and shortens the life of neutron moderator. Therefore, the barrier coating with a certain thickness and high compactness on the surface of zirconium hydride is crucial<sup>[3]</sup>. The researches on hydrogen permeation barriers mainly focus on the surface modification technique which can improve the hydrogen barrier properties of coatings. Pan et al<sup>[4]</sup> reported that the hydrogen barrier coatings can be divided into two categories: (1) using metal materials to synthesize dense compound coatings; (2) using surface treatment technique on the metal surface. The latter not only affects the performance of the zirconium hydride, but also inhibits the loss of hydrogen effectively.

The preparation techniques for hydrogen barrier coatings mainly include in situ oxidation, electroplating, spraying

technique, sol-gel, and micro-arc oxidation (MAO)<sup>[5,6]</sup>. MAO can apply on complex parts due to its simple process and high forming efficiency<sup>[7]</sup>. There are a few researches on rare earth additives in MAO electrolytes, but the influence mechanism of rare earth ions on MAO process is still unclear<sup>[8,9]</sup>. Lim et al<sup>[10]</sup> added CeO<sub>2</sub> into the silicate electrolyte during MAO for AZ31 magnesium alloys, and found that the corrosion resistance of AZ31 magnesium alloy is improved greatly. Cai et al<sup>[11]</sup> found that the corrosion resistance of magnesium alloy prepared by MAO after cerium addition is improved. Xiao et al<sup>[12]</sup> reported that the cerium can improve the surface quality of titanium alloy and the biocompatibility of ceramic coatings prepared by MAO.

The detailed research on electrolyte of MAO was presented in Ref.[13,14]. However, the reaction process and mechanism of additives in the electrolyte are still unclear. Thus, the hydrogen resistance of ceramic coatings at a constant voltage was investigated in this research.

Received date: March 25, 2021

Foundation item: National Natural Science Foundation of China (51964035); Natural Science Foundation of Inner Mongolia Autonomous Region (2019MS05020, 2020LH05017); Science and Technology Major Project of Inner Mongolia Autonomous Region (2018-810)

Corresponding author: Yan Shufang, Ph. D., Associate Professor, School of Materials Science and Engineering, Inner Mongolia University of Technology, Hohhot 010051, P. R. China, Tel: 0086-471-6575752, E-mail: ysfch@imut.edu.cn

Copyright © 2022, Northwest Institute for Nonferrous Metal Research. Published by Science Press. All rights reserved.

## 1 Experiment

The experiment material ZrH<sub>1.8</sub> (Beijing General Research Institute for Nonferrous Metals) was cut into the specimens of  $\Phi 20$  mm $\times$ 2 mm by wire cutting, and a hole of  $\Phi 3$  mm was drilled at 2 mm away from the edge of the specimen. The ZrH<sub>1.8</sub> specimens were ground by SiC abrasive papers from 360# to 1200#. Then all specimens were degreased with acetone and alcohol for 15 min, separately. After that, all the specimens were dried for MAO process.

In the phosphate electrolyte system, Na<sub>5</sub>P<sub>3</sub>O<sub>10</sub> is the main film former, while KOH, Na<sub>2</sub>(ethylene diamine tetraacetic acid) (Na<sub>2</sub>EDTA), and NaF are auxiliary film formers. Ce(NO<sub>3</sub>)<sub>3</sub>·6H<sub>2</sub>O as an electrolyte additive was added into the electrolyte with different contents of 3mol%, 6mol%, 9mol%, 12mol%, and 15mol%, separately. The main electrolyte components and parameters are shown in Table 1.

The T-MAO-B30 MAO power was used. The suspended specimen in the electrolyte was taken as the anode and the electrolytic cell was the cathode. During the MAO process of ZrH<sub>1.8</sub> alloy, the electrolyte temperature was under 17 °C by the cooling circulation system.

The thickness of coating was tested by the MiniTest-745 thickness gauge, and the phase components of the ceramic coating was characterized by X-ray diffraction (XRD). The APD automatic powder diffraction (PHILIPS, Cu target, step-scan velocity of 0.02°·s<sup>-1</sup>) was used. The QUANTA 400 environmental scanning electron microscope (SEM) was applied to observe the surface and cross-section morphologies of coatings. The element distributions were characterized by energy dispersive spectroscopy (EDS). The bonding force of coatings was tested by WS-2005 coating adhesion automatic scratch tester. The X-ray photoelectron spectroscopy (XPS) was applied to analyze the chemical valence of ceramic layers. The hydrogen resistance performance was tested by the vacuum dehydrogenation experiment. Both the uncoated and coated specimens were heated at 650 °C under the vacuum pressure of 10<sup>-4</sup> Pa for 10 h and then cooled to room temperature. Anti-permeation ability was evaluated by the permeation reduction factor (PRF), which could be calculated by Eq.(1), as follows<sup>[15,16]</sup>:

$$\text{PRF} = \frac{\Delta\omega_0}{\Delta\omega_i} \quad (1)$$

where  $\Delta\omega_i$  and  $\Delta\omega_0$  are the addition of hydrogen permeated into the ZrH<sub>1.8</sub> alloys with and without coating, respectively.

## 2 Results and Discussion

### 2.1 Surface morphology

The surface morphologies of ceramic coatings with cerium of different contents are shown in Fig. 1. It can be observed that MAO coatings have many cracks and pores when the cerium addition is 3mol%. Some large pores exist and the coating surface is extremely uneven. With increasing the cerium content, the micro-cracks on coatings are decreased. The pore size is decreased while the number of pores is increased, but the surface tends to be flat gradually, as shown in Fig. 1a~1c. The surface quality of the ceramic coating is optimally modified after MAO with 9mol% cerium, because few cracks and pores exist. With further increasing the cerium content, the ceramic coating begins to generate some micro-cracks and deposits which are synthesized at the early stage, as shown in Fig. 1d and 1e, because of the thermal stress during MAO process<sup>[17,18]</sup>. The high temperature effect during MAO process forms an instantaneous temperature difference between the high temperature coating and the low temperature electrolyte. The rapid solidification of melt due to its quenching in electrolyte leads to the decreased compactness and the rapid expansion of micro-cracks of the ceramic coatings.

Fig.2 displays the element distributions of Zr, O, and Ce of the ceramic coatings after MAO with 9mol% cerium. The surface of the ceramic coating mainly consists of Zr, O, and Ce, and Ce has an even distribution. It is indicated that Ce<sup>3+</sup> participates in the coating formation process and forms the Ce-Zr-O solid solution.

### 2.2 Cross-section morphology

The cross-section morphologies of ceramic coatings after MAO with cerium addition of different contents are shown in Fig.3. It can be observed that the ceramic coatings consist of a dense layer near the substrate and a loose layer on the outside, and there is no obvious boundaries between them. The ceramic coating is loose and porous with large pores, and the surface of the ceramic coating is irregular after MAO with 3mol% cerium. With increasing the cerium content to 6mol%, the pore size is decreased significantly, the proportion of the dense layer in the cross-section is increased, whereas an obvious crack appears between the loose layer and the dense layer. With increasing the cerium content to 9mol%, the ceramic coating surface is smooth and compact due to the high conductivity and low arc voltage of the electrolyte with cerium addition which makes the MAO process more stable and continuous. The conductivity of ions in the electrolyte is

Table 1 Electrolyte components and related parameters

Electrolyte		Forward voltage/V	Negative voltage/V	Duty cycle	Frequency/Hz	Duration/min
Component	Content/g·L <sup>-1</sup>					
Na <sub>5</sub> P <sub>3</sub> O <sub>10</sub>	18	350	120	50	100	15
KOH	15					
Na <sub>2</sub> EDTA	2					
NaF	4					

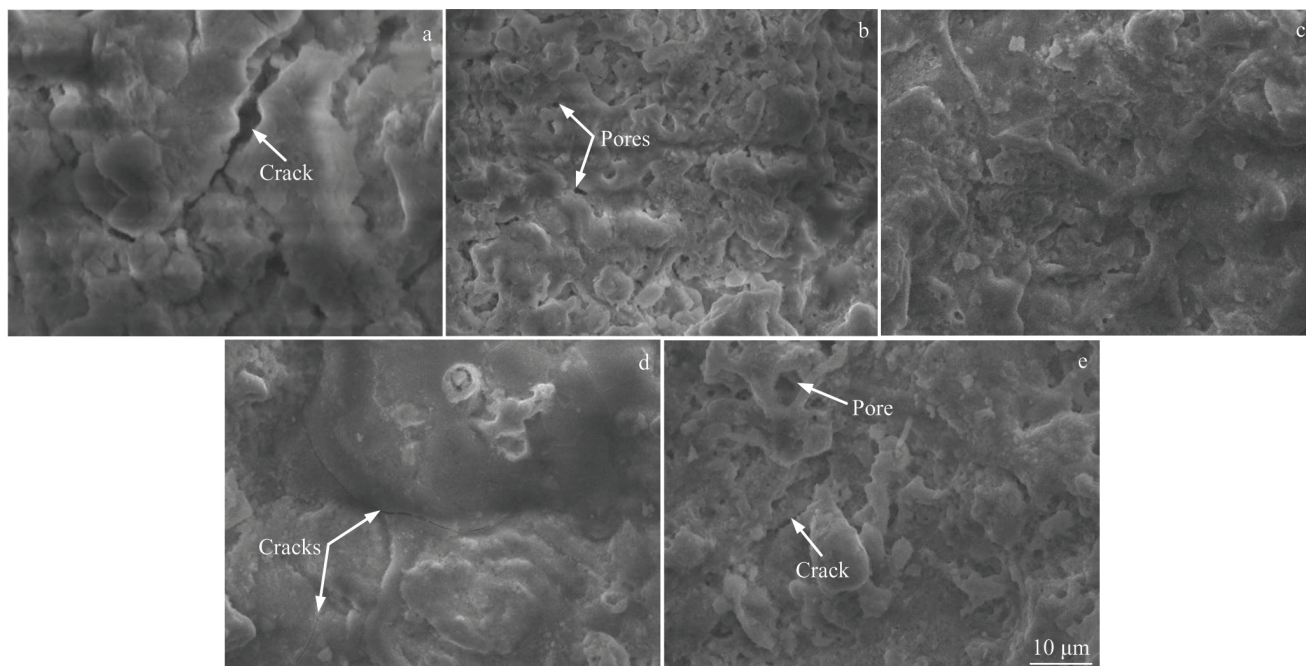


Fig.1 Surface morphologies of ceramic coatings after MAO with cerium addition of different contents: (a) 3mol%, (b) 6mol%, (c) 9mol%, (d) 12mol%, and (e) 15mol%

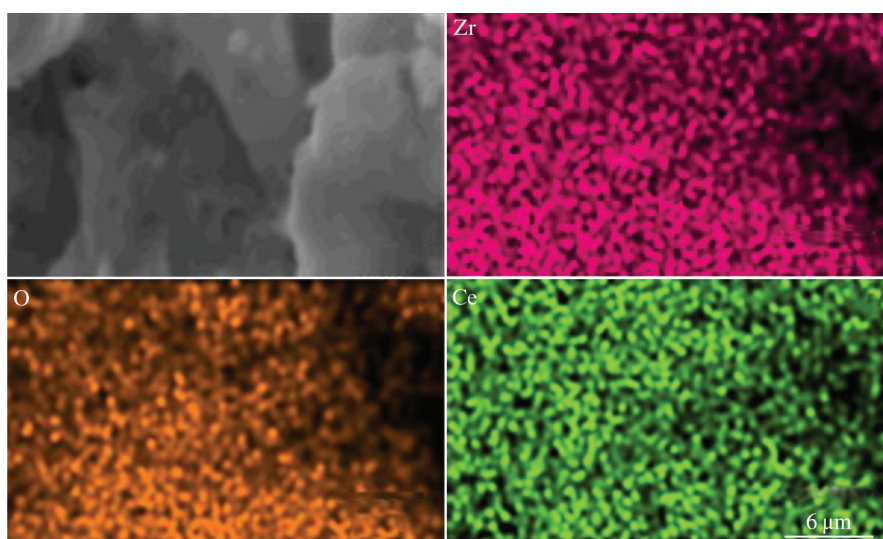


Fig.2 EDS analysis of ceramic coating after MAO with 9mol% cerium addition

enhanced rapidly with increasing the cerium content, which accelerates the growth of the ceramic coatings and increases the breakdown threshold of ceramic coating surface simultaneously. Therefore, the large cracks and pores appear on the formed coatings, which reduces the density of the ceramic coating, as shown in Fig.3d and 3e.

### 2.3 Bonding strength

Fig.4 shows the bonding strength of ceramic coatings after MAO with cerium addition of different contents. It can be seen that with increasing the cerium content, the bonding strength is decreased generally. When the cerium content is 3mol%, the bonding strength reaches the maximum of 84.39

N, whereas the minimum bonding strength is obtained when the cerium content is 15mol%. When the cerium content is 9mol%, the bonding strength is 52.46 N owing to the increase in thickness of ceramic coatings, which results in the brittleness rise, thereby increasing the cracks in the ceramic coatings<sup>[19]</sup>. During MAO process, the coating growth at later period can mainly generate the loose layer rather than the dense layer. Therefore, the bonding strength is decreased with further increasing the thickness of ceramic coating, i. e., the bonding strength is decreased with increasing the cerium content from 9mol% to 15mol%.

### 2.4 Phase components

XRD patterns of ceramic coatings after MAO with cerium

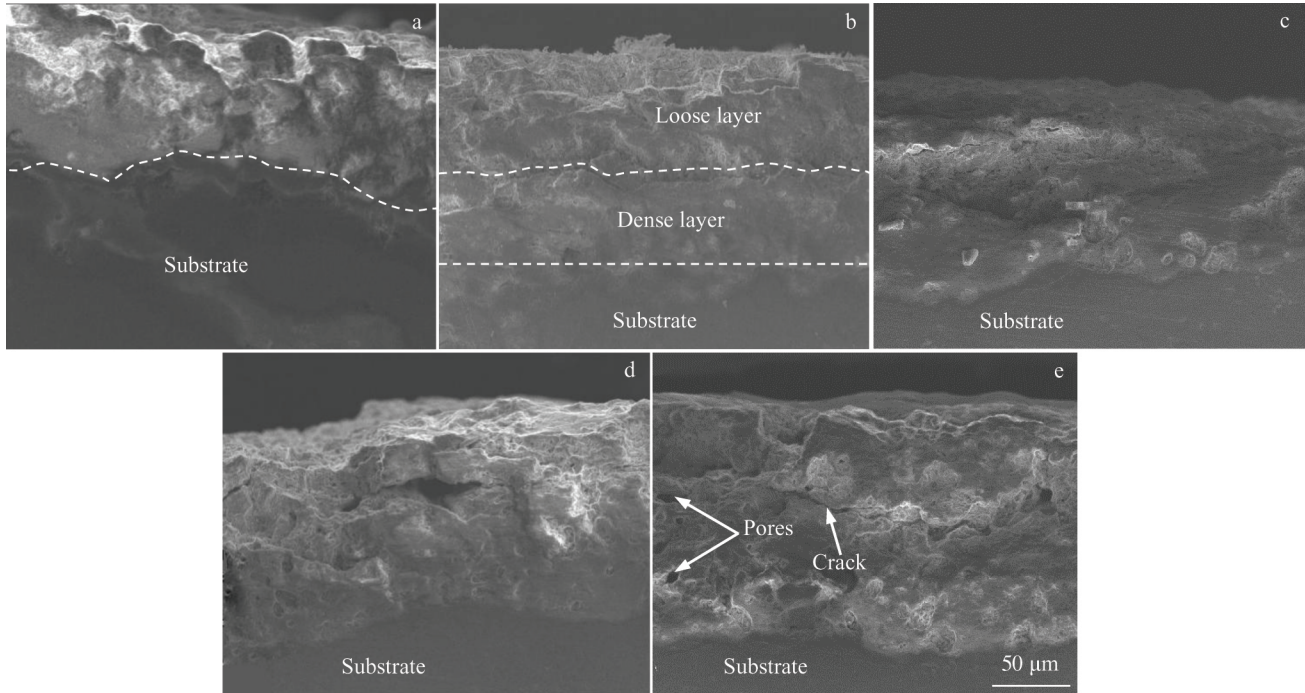


Fig.3 Cross-section morphologies of ceramic coatings after MAO with cerium addition of different contents: (a) 3mol%, (b) 6mol%, (c) 9mol%, (d) 12mol%, and (e) 15mol%

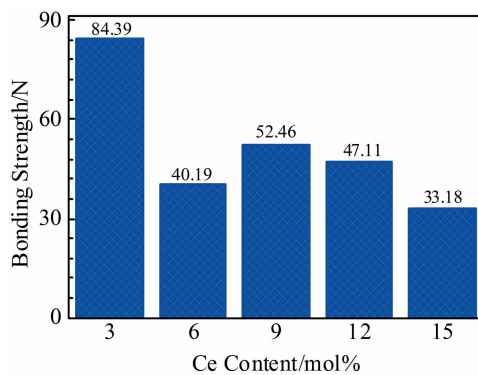


Fig.4 Bonding strengths of ceramic coatings after MAO with cerium addition of different contents

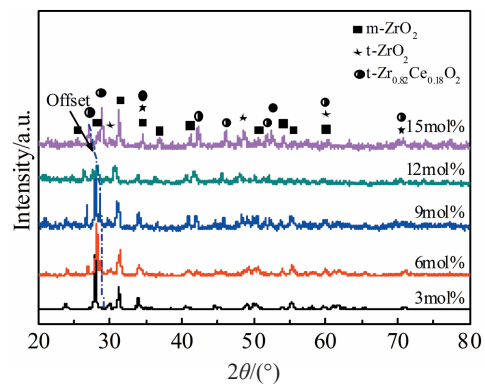


Fig.5 XRD patterns of ceramic coatings after MAO with cerium addition of different contents

addition of different contents are shown in Fig. 5. It is found that the ceramic coating is mainly composed of  $m\text{-ZrO}_2$ ,  $t\text{-ZrO}_2$ , and  $t\text{-Zr}_{0.82}\text{Ce}_{0.18}\text{O}_2$ . The variance of cerium content has no obvious effect on the phase components of the ceramic coatings. However, with increasing the cerium content, the intensity of  $m\text{-ZrO}_2$  diffraction peak is weakened gradually, whereas that of  $t\text{-ZrO}_2$  diffraction peak is strengthened gradually. The new solid-solution phase  $t\text{-Zr}_{0.82}\text{Ce}_{0.18}\text{O}_2$  appears when the cerium content is 6mol% , and its intensity is gradually increased with further increasing the cerium content.

Table 2 illustrates the relative contents of each phase in the ceramic coatings, which are calculated by the K-Value method of XRD results. The ceramic coating is mainly composed of  $m\text{-ZrO}_2$ . With increasing the cerium content, the content of  $m\text{-ZrO}_2$  is decreased, while that of  $t\text{-Zr}_{0.82}\text{Ce}_{0.18}\text{O}_2$  is increased.

**Table 2** Relative content of phases in ceramic coatings after MAO with cerium addition of different contents

Ce content/mol%	3	6	9	12	15
$m\text{-ZrO}_2$ content/wt%	94.0	79.3	76.9	75.8	74.7
$t\text{-ZrO}_2$ content/wt%	4.0	8.1	8.7	9.3	9.3
$t\text{-Zr}_{0.82}\text{Ce}_{0.18}\text{O}_2$ content/wt%	2.0	12.6	14.4	14.9	16.0

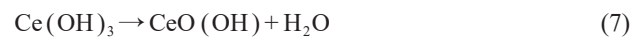
It can be found that the content of  $t\text{-ZrO}_2$  is basically unchanged when the cerium content is 12mol%~15mol% . Thus, it can be concluded that the  $m\text{-ZrO}_2$  is mainly converted to  $t\text{-Zr}_{0.82}\text{Ce}_{0.18}\text{O}_2$ . Moreover, according to Fig. 5, the  $\text{ZrO}_2$  diffraction peak shifts towards the small angle area as the cerium content increases. It is indicated that the ceria-containing large grain phases are dissolved and transformed

into the zirconia-containing small grain phases, which generates an oxygen vacancy of zirconia. Thus, the phase transition from *t*-ZrO<sub>2</sub> to *m*-ZrO<sub>2</sub> is inhibited during MAO process, and the metastable *t*-ZrO<sub>2</sub> exists at room temperature and generates the ceria-stabilized zirconia (CSZ) composite coatings. The cerium addition is beneficial to the formation of stable multi-phases of Ce-Zr-O composite coating, thereby ameliorating the performance of zirconium hydride at service temperatures above 600 °C.

### 2.5 Coating components

XPS spectra of the ceramic coatings after MAO with 9mol% cerium are shown in Fig. 6, revealing the chemical valence of different elements of ceramic coatings. The ceramic coating surface is mainly composed of Zr, O, and Ce elements, and contains a small amount of Na, F, and P. According to Fig. 6b, the Zr 3d has two characteristic peaks. The peak with binding energy of 182.28 eV is at the position of Zr 3d<sub>5/2</sub>, corresponding to ZrO<sub>2</sub>. It is also found that the peak with binding energy of 185.3 eV is at the position of Zr 3d<sub>3/2</sub>, corresponding to ZrO<sub>2</sub>. O 1s has two characteristic peaks: the peak with binding energy of 530.73 eV corresponds to ZrO<sub>2</sub> (529.9 eV), and the other of 532.27 eV corresponds to O-H (532.4 eV) which may form Zr(OH)<sub>4</sub> and CeO(OH) with Zr and Ce elements, respectively. Ce 3d<sub>5/2</sub> has two characteristic peaks: the peak with binding energy of 882.44 eV corresponds to CeO<sub>2</sub> (882 eV) and the other one of 884.82 eV corresponds to the cerium oxide. It can be concluded that the Zr, O, and Ce elements on the ceramic coating surface mainly exist as Ce-Zr oxides, which is in agreement with the results of XRD and EDS analyses for ZrO<sub>2</sub> and Zr<sub>0.82</sub>Ce<sub>0.18</sub>O<sub>2</sub>.

The detailed reactions during MAO in this research are presented as follows:



The Zr<sup>4+</sup> in Eq. (3) is derived from the ZrH<sub>1.8</sub> substrate. A strong electric field is formed between the ZrH<sub>1.8</sub> and electrolytic cell, thereby ionizing the zirconium hydride into Zr<sup>4+</sup> in the electrolyte. Meanwhile, the OH<sup>-</sup> undergoes a series of chemical reactions on the cathode to produce Zr(OH)<sub>4</sub> precipitates, metastable Ce(OH)<sub>3</sub>, and H<sub>2</sub><sup>[20]</sup>. With the MAO process proceeding, the multi-discharge phenomenon occurs on the ZrH<sub>1.8</sub> alloy surface. The instantaneous temperature of melt can reach thousands degree of Kelvin, which reduces the solubility of Ce(OH)<sub>3</sub> and dehydration of Ce(OH)<sub>3</sub> to form CeO(OH) (Eq. (7)). However, the metastable Ce(OH)<sub>3</sub> and CeO(OH) are very unstable. These precipitations are oxidized to Ce(OH)<sub>4</sub> quickly (Eq. (8)). The migration rate of ions in the electrolyte is accelerated after the cerium addition. Meanwhile, the energy is concentrated on the interface between the coating and the electrolyte, so the hydroxides, such as Zr(OH)<sub>4</sub> and Ce(OH)<sub>4</sub>, are deposited in the discharge channels with the

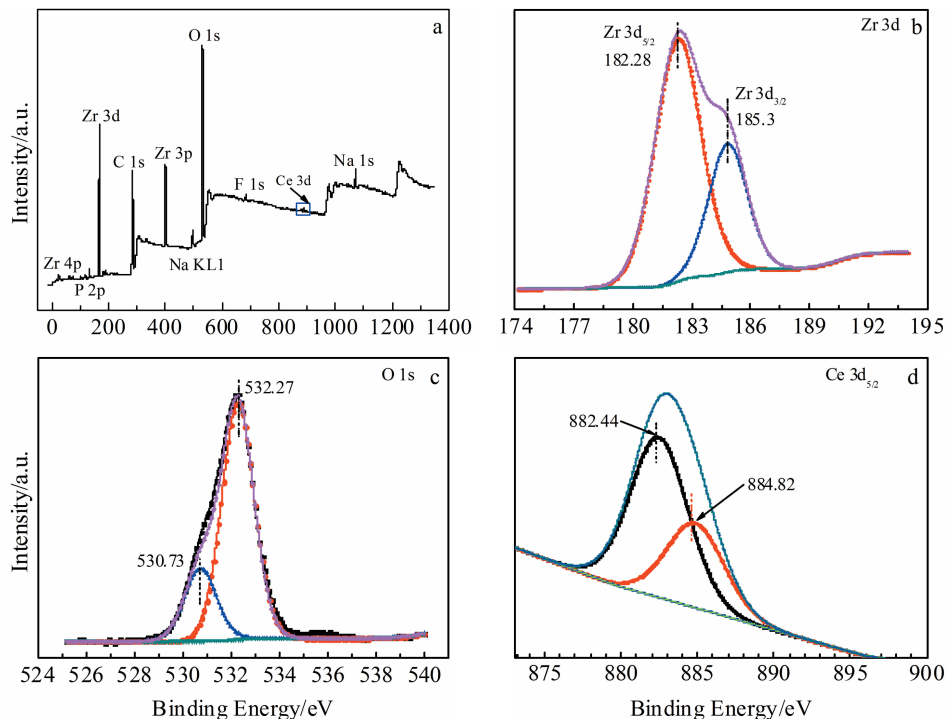


Fig.6 XPS spectra of ceramic coatings after MAO with 9mol% cerium: (a) total spectrum; (b) Zr 3d; (c) O 1s; (d) Ce 3d<sub>5/2</sub>

electrophoresis.  $Zr(OH)_4$  and  $Ce(OH)_4$  are converted into crystal  $ZrO_2$  and  $CeO_2$  by plasma chemistry, thermal decomposition, and reactions in the discharge channels under high temperature and high pressure<sup>[21]</sup> (Eq. (9) and Eq. (10)). Ceria and zirconia have the similar thermal expansion coefficients and they can jointly form a wide tetragonal phase solid solution zone. Based on this character, the temperature of martensite transformation ( $t\text{-}ZrO_2 \rightarrow m\text{-}ZrO_2$ ) is reduced greatly, which is beneficial to the production of CSZ coatings.

### 2.6 Thickness and hydrogen resistance of coatings

The relationship between the coating thickness and hydrogen PRF of the ceramic coating prepared by MAO with cerium of different contents is shown in Fig.7. It indicates that with increasing the cerium content from 0mol% to 9mol%, the coating thickness and the hydrogen PRF are increased gradually. With further increasing the cerium content, the hydrogen PRF is decreased. In brief, the hydrogen resistance permeation ability of ceramic coatings after MAO is greatly improved compared with that of bare  $ZrH_{1.8}$ , and it is increased firstly and then decreased with increasing the cerium content in MAO process. This is because the high chemical activity of  $Ce^{3+}$  can promote the ionization of various components in the electrolyte<sup>[22]</sup>. With increasing the cerium content, the ion transport process is further accelerated in the electrolyte and the plasma physicochemical reactions in the discharge channels are intensified, which promotes the formation of ceramic coatings. The ceramic coating has an optimal hydrogen resistance performance after MAO with 9mol% cerium: its hydrogen PRF achieves the maximum of 19. It can be concluded that the cerium addition can uniformly promote the electrochemical and thermochemical plasma reactions. The mechanical interlocking between the coating and substrate increases the proportion of dense layer, so the hydrogen resistance performance of the ceramic coatings is improved. According to Fig.1d, 1e, Fig.3d, and 3e, the coating thickness is increased with increasing the cerium content from 12mol% to 15mol%. But there are obvious cracks appear on the ceramic coatings, which decreases the hydrogen resistance performance of ceramic coatings.

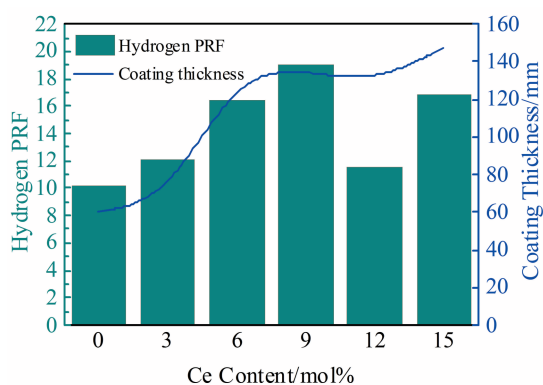


Fig.7 Coating thickness and hydrogen PRF of ceramic coatings after MAO with cerium addition of different contents

## 3 Conclusions

1) The ceria-stabilized zirconia coating with good hydrogen resistance permeation can be prepared by micro-arc oxidation with cerium addition. The ceramic coating consists of a loose layer on the outside and a dense layer near the  $ZrH_{1.8}$  substrate. With increasing the cerium content from 3mol% to 15mol%, the thickness of ceramic coatings is increased gradually while the bonding strength is mainly decreased. When the cerium content is 9mol%, the ceramic coating has the optimal bonding strength and thickness.

2) The ceramic coating is mainly composed of  $m\text{-}ZrO_2$ ,  $t\text{-}ZrO_2$ , and  $t\text{-}Zr_{0.82}Ce_{0.18}O_2$ . The cerium addition promotes the formation of stable  $t\text{-}ZrO_2$  at high temperature and inhibits the phase transformation of zirconia. When the cerium content is 9mol%, the ceramic coating is uniform and dense with few defects, such as cracks and pores. Meanwhile, the ceramic coating has good hydrogen resistance ability with the maximum hydrogen permeation reduction factor of 19.

## References

- 1 Wang Zhigang, Chen Weidong, Yan Shufang et al. *Rare Metal Materials and Engineering*[J], 2015, 44(1): 184 (in Chinese)
- 2 Ponomarev-Stepnoi N N, Bubelev V G, Glushkov Y S. *Nuclear Science & Engineering*[J] 1995, 119(2): 108
- 3 Yan Guoqing, Chen Weidong, Fan Xiujuan et al. *Rare Metal Materials and Engineering*[J], 2015, 44(2): 447 (in Chinese)
- 4 Pan Xiaoxia, Tan Yun, Feng Jie et al. *Surface Technology*[J], 2000, 29(3): 13 (in Chinese)
- 5 Li Shijiang, Yan Shufang, Chen Weidong et al. *Rare Metals*[J], 2019, 43(8): 831 (in Chinese)
- 6 Yao Z, Suzuki A, Levchuk D et al. *Journal of Nuclear Materials* [J], 2009, 386-388: 700
- 7 Krishtal M M. *Metal Science & Heat Treatment*[J], 2004, 46(9-10): 377
- 8 Li Shijiang, Yan Shufang, Zhong Xuekui et al. *Surface Technology*[J], 2019, 48(4): 279 (in Chinese)
- 9 Rudnev V S, Yarovaya T P, Boguta D L et al. *Journal of Electroanalytical Chemistry*[J], 2001, 497(1): 150
- 10 Lim T S, Ryu H S, Hong S H. *Corrosion Science*[J], 2012, 62: 104
- 11 Cai Jingshun, Cao Fahe, Chang Linrong et al. *Journal of Zhejiang University of Science*[J], 2011, 45(11): 2055 (in Chinese)
- 12 Xiao Lairong, Xu Liangliang, Yi Danqing et al. *Rare Metals*[J], 2008, 27(3): 257 (in Chinese)
- 13 Yan Shufang, Liu Xiangdong, Chen Weidong et al. *Rare Metal Materials and Engineering*[J], 2014, 43(7): 1717 (in Chinese)
- 14 Zhang P F, Yan S F, Chen W D et al. *Journal of Inorganic Materials*[J], 2018, 33(3): 284
- 15 Yan Guoqing. *Thesis for Doctorate*[D]. Beijing: General Research Institute for Nonferrous Metals, 2017 (in Chinese)
- 16 Nakamichi M, Kawamura H, Teratani T. *Journal of Nuclear*

- 17 Wang Zhigang, Chen Weidong, Yan Shufang et al. *Rare Metal Materials and Engineering*[J], 2015, 44(3): 718 (in Chinese)
- 18 Liu H L, Wang B, Qi Z W et al. *Rare Metal Materials and Engineering*[J], 2018, 47(11): 3338
- 19 Ao N, Liu D X, Zhang X H et al. *Journal of Alloys and Compounds*[J], 2020, 823: 153 823
- 20 Yang X Z, He Y D, Wang D R et al. *Chinese Science Bulletin*[J], 2003, 48(8): 746
- 21 Tang M Q, Li W P, Liu H C et al. *Applied Surface Science*[J], 2012, 258(15): 5869
- 22 Mohedano M, Perez P, Matykina E et al. *Surface & Coatings Technology*[J], 2020, 383: 125 253

## 铈浓度对 $ZrH_{1.8}$ 微弧氧化膜层阻氢性能的影响

李世江<sup>1</sup>, 闫淑芳<sup>1</sup>, 陈伟东<sup>1,2</sup>, 马文<sup>1,2</sup>

(1. 内蒙古工业大学 材料科学与工程学院, 内蒙古 呼和浩特 010051)

(2. 内蒙古自治区薄膜与涂层重点实验室, 内蒙古 呼和浩特 010051)

**摘要:** 利用微弧氧化技术在电解液中加入不同含量的铈, 制备了阻氢性能良好的二氧化铈稳定氧化锆 (ceria-stabilized zirconia, CSZ) 陶瓷膜。利用涂层测厚仪、涂层附着力自动划痕仪、扫描电子显微镜、X射线能谱仪、X射线衍射仪、X射线光电子能谱仪和真空脱氢实验对膜层的厚度、结合力、形貌、相结构、元素化学价态和膜层的阻氢性能进行了测试和表征。结果表明: CSZ陶瓷膜主要由单斜相氧化锆 ( $m\text{-ZrO}_2$ )、四方相氧化锆 ( $t\text{-ZrO}_2$ ) 和  $t\text{-Zr}_{0.82}\text{Ce}_{0.18}\text{O}_2$  组成。随铈浓度的增加, 膜层厚度逐渐增加。当铈浓度为 9mol% 时, 陶瓷膜厚度为 135.5  $\mu\text{m}$ , 结合力为 52.46 N, 膜层具有优异的阻氢性能, 阻氢渗透因子为 19。铈的加入抑制了  $t\text{-ZrO}_2$  向  $m\text{-ZrO}_2$  的相转变, 促进了高温稳定  $t\text{-ZrO}_2$  的生成。

**关键词:** 氧化锆; 微弧氧化; 铈浓度; 阻氢渗透因子

作者简介: 李世江, 男, 1991年生, 硕士, 内蒙古工业大学材料科学与工程学院, 内蒙古 呼和浩特 010051, 电话: 0471-6575752, E-mail: lishijiang2016@163.com